



Article

Super-Twisting Algorithm Backstepping Adaptive Terminal Sliding-Mode Tracking Control of Quadrotor Drones Subjected to Faults and Disturbances

Ye Zhang ^{1,2} , Yihao Fu ¹, Zhiguo Han ^{1,*} and Jingyu Wang ¹ 

¹ School of Astronautics, Northwestern Polytechnical University, Xi'an 710072, China; zhang_ye@nwpu.edu.cn (Y.Z.); fyhao@mail.nwpu.edu.cn (Y.F.); jywang@nwpu.edu.cn (J.W.)

² National Key Laboratory of Air-Based Information Perception and Fusion, Luoyang 471009, China

* Correspondence: zghan2017@nwpu.edu.cn

Abstract: The rapid advancement of quadrotor systems has introduced significant challenges across multiple disciplines. Among these, fault tolerance and trajectory tracking in complex environments have long been recognized as critical challenges in quadrotor control research. To address issues such as rotor performance degradation and external disturbances, a novel position-attitude control system was developed, aimed to achieve precise position and attitude tracking. Initially, a dynamic model of the quadrotor was formulated, serving as the foundation for the controller design. Super-twisting algorithm terminal sliding-mode control (STATSMC) was then employed within the position loop to suppress chattering by the super-twisting algorithm. Subsequently, a new super-twisting algorithm backstepping adaptive terminal sliding-mode control (STABATSMC) was proposed to mitigate the controller output and merge enable adherence to the desired Euler angles in case of failure. This approach enables the quadrotor to accurately follow position commands and achieve the desired attitude angles. The introduction of terminal sliding-mode control enhances convergence speed and tracking precision, while the super-twisting algorithm mitigates chattering and smoothens the control output. Finally, a series of simulation experiments were conducted within the Simulink environment to validate the proposed control system. The experimental results are compared with the state-of-art terminal sliding-mode control method, demonstrating the superior performance and effectiveness of the proposed method.

Keywords: quadrotor drones; trajectory tracking; super-twisting algorithm; sliding-mode control; multiple interference



Academic Editor: Agostino De Marco

Received: 12 December 2024

Revised: 12 January 2025

Accepted: 15 January 2025

Published: 22 January 2025

Citation: Zhang, Y.; Fu, Y.; Han, Z.; Wang, J. Super-Twisting Algorithm Backstepping Adaptive Terminal Sliding-Mode Tracking Control of Quadrotor Drones Subjected to Faults and Disturbances. *Drones* **2025**, *9*, 82. <https://doi.org/10.3390/drones9020082>

Copyright: © 2025 by the authors. Licensee MDPI, Basel, Switzerland. This article is an open access article distributed under the terms and conditions of the Creative Commons Attribution (CC BY) license (<https://creativecommons.org/licenses/by/4.0/>).

1. Introduction

In recent years, micro aerial vehicles (MAVs), especially quadrotor drones, have gained popularity due to their small size, maneuverability, and low cost [1–3]. These qualities make them highly suitable for performing tasks in complex terrains and environments in place of humans, such as military reconnaissance, agricultural monitoring, civilian aerial photography, and formation performances [4–6]. In [7], a method combining UAV and the Internet of Things (IoT) is proposed for the health monitoring of bridges. In [8], a new method of synchronization and data collection using Bluetooth Low Energy (BLE) is proposed for bridge structural health monitoring by UAVs. Sun et al. used multiple UAVs to achieve fast and safe operation of rigid body payload attitude [9]. With the widespread application of MAVs, ensuring their operational safety has become a key research focus [10–13]. The high dependency on flight control systems [14–21] and the lacking and redundant

structures makes the control of quadrotor drones highly sensitive to changes in the external environment and faults. Consequently, designing a robust and high-precision fault-tolerant control system is critical for enhancing their adaptability to complex environments and external disturbances, ensuring the safe and reliable operation of various missions [22].

The fault-tolerant control of quadrotors has become a prominent research area. Classical control theories face challenges in achieving high-quality control of these vehicles. Guo et al. [23] proposed a quadrotor anti-interference control scheme based on multiple observers that can effectively deal with the payload interference and wind interference. Omid Mofid et al. [24] designed an adaptive backstepping global sliding-mode control method, which considers input delay, model uncertainty, and wind disturbance to achieve fast response. In [25], a disturbance observer-based controller (DOBC) was designed for a quadrotor engine to deal with gusts in flight by estimating and attenuating external wind disturbances. In addition, a nonlinear extended state observer is designed for the inner loop subsystem [26] of the quadrotor, which enables the system to achieve attitude stability when a unilateral load is suspended. In [27], a nonlinear robust controller is designed based on the nonlinear disturbance observer. This observer estimates the external disturbances of the quadrotor and solves the nonlinear robust control problem for point-tracking of the quadrotor. While these approaches have demonstrated effectiveness, they involve complex design processes and stringent assumptions. Given the relatively low cost of quadrotors, it is preferable to develop fault-tolerant control systems that are as simple and efficient as possible.

Sliding-mode control (SMC) has been widely used in fault-tolerant control fields, such as robot operation [28], linear motor positioning [29], and underwater robots [30]. Because of its strong robustness, fast response, and insensitivity to uncertainty and interference, related research has been conducted by scholars locally and abroad. The traditional sliding-mode control cannot guarantee the convergence time of the control system [31], and the terminal sliding-mode control (TSMC) can ensure the rapid convergence of the system [32]. In [33], the quadrotor system is divided into an inner loop and an outer loop. Non-singular terminal sliding-mode control (NTSMC) is used to converge to the desired position and attitude in finite time. In [34], Jiao et al. proposed a new adaptive backstepping fast non-singular integral terminal sliding-mode control (ABFNITSMC), which is applied to the attitude control loop of the UAV to ensure finite-time convergence of the quadrotor to the desired Euler angle. This system has high robustness under the model uncertainties and external disturbances. Although TSMC can ensure the convergence of the system in finite time, there is a more severe chattering phenomenon, which affects the control accuracy of the system, increases the energy consumption of the system, and even causes damage to the components in the system. At present, chattering suppression has become a key research direction. Super-twisting algorithm is widely used in motor speed control, attitude control, and other fields, which can effectively suppress the phenomenon of jiggling [35–39]. In [35], in order to overcome the chattering phenomenon in sliding-mode control and make the flight more stable, an Adaptive Superhelix algorithm (ASTA) controller was introduced. Zhang et al. [36] proposed a super-twisted non-singular fast terminal sliding-mode control law for the attitude control of a fixed-wing UAV, which can effectively suppress the disturbance and weaken the flutter. Compared with the fixed-wing UAV, the quadrotor controls the attitude through rotor speed, which puts forward higher requirements on the anti-damage ability of the attitude controller. By introducing superspiral control on the basis of non-singular terminal sliding-mode control, the chattering problem can be effectively suppressed while ensuring high tracking accuracy.

In order to achieve fast and accurate tracking of position and attitude for unmanned aerial vehicles (UAVs), this paper combines terminal sliding-mode control with backstep-

ping control and super-twisting algorithm, and finally enhances the robustness of the controller through an adaptive control law. A novel controller based on super-twisting algorithm backstepping adaptive terminal sliding-mode control (STABATSMC) is designed. The main contributions of this paper are as follows:

1. A novel position–attitude control scheme is developed for quadrotor drones affected by external disturbances and faults.
2. The proposed STABATSMC control demonstrates strong robustness against nonlinearities, abrupt faults, and external disturbances. Compared with traditional control methods, it offers faster convergence and more precise tracking performance while eliminating system chattering.
3. The stability proof of the quadrotor’s trajectory tracking and attitude control system is provided based on Lyapunov’s theory.

The structure of this paper is organized as follows: Section 2 derives the dynamic model of the quadrotor. Section 3 presents the expressions for the terminal sliding-mode control and super-twisting terminal sliding-mode control used in the position and attitude control loops, and proves the stability of the control system using Lyapunov’s theory. Additionally, a rotor speed allocation scheme is provided. In Section 4, simulation results are presented, followed by conclusions and future research directions in Section 5.

2. Dynamic Model of Quadrotors

A schematic diagram of the quadrotor used in the experiment is shown in Figure 1. The UAV is an underactuated system, with the vector $P = (X, Y, Z)^T$ representing the position of the UAV, and the vector $P = (\Phi, \Theta, \Psi)^T$ representing the quadrotor’s attitude angles.

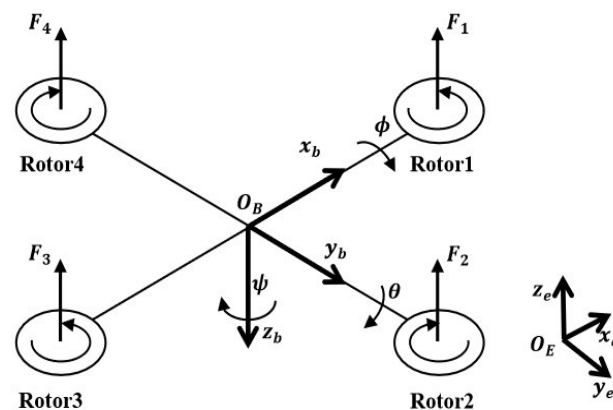


Figure 1. The model of the quadrotor.

For modeling convenience, this paper introduces the Ground Inertial Frame $S_e : (O_E, x_e, y_e, z_e)$ and the body frame $S_b : (O_B, x_b, y_b, z_b)$ to describe the 6-DOF model of the quadrotor.

In the frame S_b , the origin O_B coincides with the center of mass of the quadrotor. The rotational speeds of the quadrotor’s rotors are denoted by $\tilde{\omega} = (\tilde{\omega}_1, \tilde{\omega}_2, \tilde{\omega}_3, \tilde{\omega}_4)^T$. The coordinates $x, y,$ and z represent the quadrotor’s displacement in the lateral, longitudinal, and vertical directions in the inertial frame S_b , respectively. The angles $\Phi, \Theta,$ and Ψ represent the roll, pitch, and yaw rotations of the quadrotor in the body frame. The model of the system can be expressed as follows:

$$m\ddot{P} = F_A + F_G + f + F_D \tag{1}$$

$$J\dot{\omega} = -\omega \times J\omega + M_L + M_f \tag{2}$$

where P represents the position of the UAV in the inertial frame.

$$P = \begin{bmatrix} x \\ y \\ z \end{bmatrix} \quad (3)$$

where F_A represents the aerodynamic forces acting on the UAV in the inertial frame.

$$F_A = R_b^e \begin{bmatrix} 0 \\ 0 \\ -T \end{bmatrix} \quad (4)$$

where T_i represents the thrust produced by the i -th rotor of the UAV and C_T denotes the thrust coefficient of the rotor.

$$T = \sum_{i=1}^4 T_i = \sum_{i=1}^4 C_T \tilde{\omega}_i^2 \quad (5)$$

where R_b^e is the transformation matrix from S_b to S_e ; F_G represents the gravitational force acting on the quadrotor; F_D represents the internal unmodelable parts and external disturbances of the quadrotor; and f denotes the aerodynamic drag experienced by the quadrotor during flight.

$$F_D = \begin{bmatrix} d_x \\ d_y \\ d_z \end{bmatrix} \quad (6)$$

$$f = C_f \begin{bmatrix} \dot{x} \\ \dot{y} \\ \dot{z} \end{bmatrix} \quad (7)$$

where C_f denotes the drag coefficient of the quadrotor; J represents the moment of inertia matrix of the quadrotor, and it can be described as a diagonal matrix, according to the following assumption:

$$J = \text{diag}(J_{xx}, J_{yy}, J_{zz}) \quad (8)$$

where Ω represents the rotational angular velocity of the quadrotor in the body frame S_b .

$$\Omega = \begin{bmatrix} p \\ q \\ r \end{bmatrix} \quad (9)$$

where M_L denotes the sum of the lift torques generated by the four rotors of the quadrotor, and M_f is the reaction torque generated by the air resistance on the rotor. Yaw motion of the quadrotor is caused when the torques generated by the two sets of rotors of the aircraft are not equal. d denotes the distance from each rotor to the center of gravity of the quadrotor C_M and represents the torque coefficient caused by air drag.

$$M_L = \begin{bmatrix} M_{Lx} \\ M_{Ly} \\ M_{Lz} \end{bmatrix} = \begin{bmatrix} d(T_4 - T_2) \\ d(T_3 - T_1) \\ 0 \end{bmatrix} \quad (10)$$

$$M_f = \begin{bmatrix} 0 \\ 0 \\ \sum_{i=1}^4 (-1)^i C_M \tilde{\omega}_i^2 \end{bmatrix} \quad (11)$$

The relationship between the attitude angle's rate $\dot{\Theta}$ in the inertial frame S_e and the angular velocity $\dot{\Omega}$ in the body frame S_b is given by

$$\dot{\Theta} = W\dot{\Omega} \quad (12)$$

then,

$$\begin{bmatrix} \dot{\phi} \\ \dot{\theta} \\ \dot{\psi} \end{bmatrix} = \begin{bmatrix} 1 & \tan \theta \sin \phi & \tan \theta \cos \phi \\ 0 & \cos \phi & -\sin \phi \\ 0 & \sin \phi / \cos \theta & \cos \phi / \cos \theta \end{bmatrix} \begin{bmatrix} p \\ q \\ r \end{bmatrix} \quad (13)$$

Based on the small-angle approximation principle, the transformation matrix W can be approximated as the identity matrix:

$$\begin{bmatrix} \dot{\phi} \\ \dot{\theta} \\ \dot{\psi} \end{bmatrix} \approx \begin{bmatrix} p \\ q \\ r \end{bmatrix} \quad (14)$$

The complete nonlinear equations for the quadrotor are given by

$$\begin{bmatrix} \dot{x} \\ \dot{y} \\ \dot{z} \\ \dot{v}_x \\ \dot{v}_y \\ \dot{v}_z \\ \dot{\phi} \\ \dot{\theta} \\ \dot{\psi} \\ \dot{p} \\ \dot{q} \\ \dot{r} \end{bmatrix} = \begin{bmatrix} v_x \\ v_y \\ v_z \\ \frac{T}{m} (\sin \psi \sin \phi + \cos \psi \cos \phi \sin \theta) - \frac{C_f}{m} \dot{x} + d_x \\ \frac{T}{m} (\sin \psi \sin \theta \cos \phi - \cos \psi \sin \phi) - \frac{C_f}{m} \dot{y} + d_y \\ \frac{T}{m} (\cos \theta \cos \phi) - g - \frac{C_f}{m} \dot{z} + d_z \\ p \\ q \\ r \\ qr \left(\frac{J_{yy} - J_{zz}}{J_{xx}} \right) + \frac{M_x}{J_{xx}} \\ pr \left(\frac{J_{zz} - J_{xx}}{J_{yy}} \right) + \frac{M_y}{J_{yy}} \\ pq \left(\frac{J_{xx} - J_{yy}}{J_{zz}} \right) + \frac{M_z}{J_{zz}} \end{bmatrix} \quad (15)$$

3. Control System Design

This section focuses on the design of trajectory tracking control strategies and stability analysis. Given the challenges posed by model uncertainties, sudden faults, and external disturbances in complex environments, a trajectory tracking control strategy is formulated to ensure rapid and accurate tracking of the reference commands. To achieve this goal and effectively mitigate chattering, a novel control scheme is proposed that combines super-twisting sliding-mode control with non-singular terminal sliding-mode control. This approach ensures that the UAV can quickly and accurately track the desired trajectory and attitude angles, while avoiding control failure issues associated with singularities. The integral term introduced in the super-twisting algorithm sliding-mode control effectively suppresses chattering during flight. The control loop we designed for this quadrotor is shown in Figure 2.

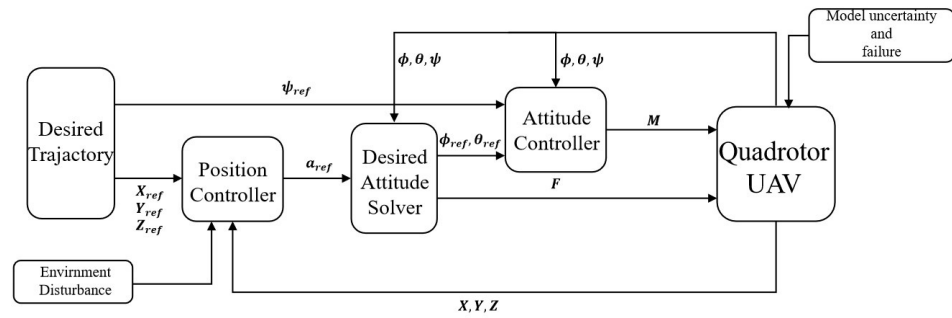


Figure 2. Control loop of the quadrotor.

3.1. Position Control System

The super-twisting algorithm terminal sliding-mode control (STATSMC) exhibits excellent robustness. It combines the features of super-twisting control and terminal sliding-mode control to achieve precise trajectory tracking and stable attitude control while effectively mitigating chattering during flight. Terminal sliding-mode control ensures accurate tracking of commands, but it often suffers from high-frequency oscillations and significant amplitude fluctuations, which can negatively impact attitude loop tracking and induce chattering. The super-twisting algorithm, by incorporating an integral term, effectively suppresses chattering and enhances the system’s robustness.

The quadrotor’s position control loop is illustrated in Figure 3. To address both tracking accuracy and responsiveness, STATSMC is used for tracking the trajectory in the x and y directions, while TSMC is employed for the z direction.

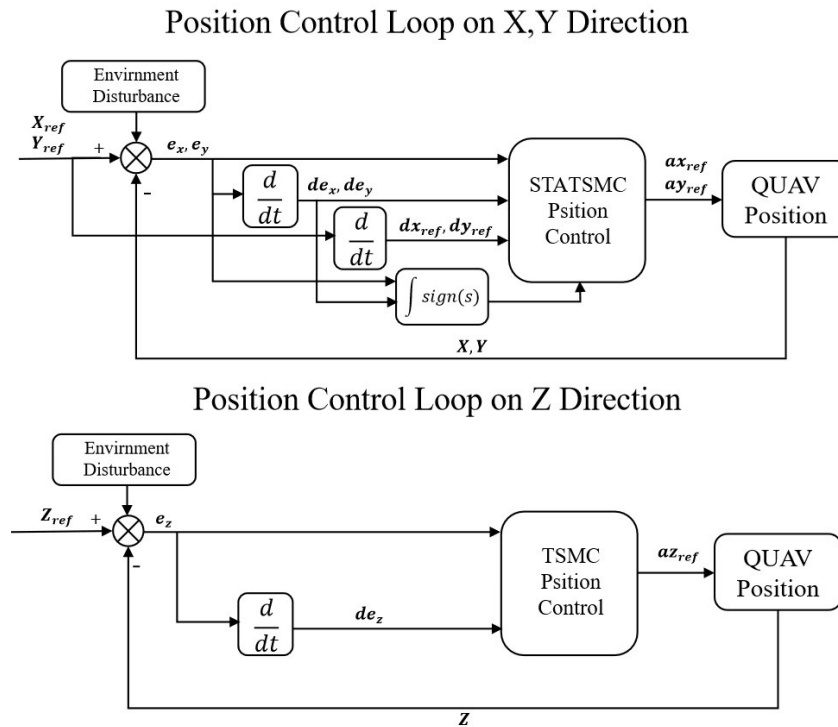


Figure 3. Position control loop of the quadrotor.

The position tracking error is defined as

$$\begin{bmatrix} e_x \\ e_y \\ e_z \end{bmatrix} = \begin{bmatrix} x - x_{ref} \\ y - y_{ref} \\ z - z_{ref} \end{bmatrix} \tag{16}$$

where, x_{ref} , y_{ref} , and z_{ref} represent the desired trajectories in the x , y , and z directions, respectively. The position tracking error can be expressed as

$$\begin{bmatrix} de_x \\ de_y \\ de_z \end{bmatrix} = \begin{bmatrix} \dot{x} - \dot{x}_{ref} \\ \dot{y} - \dot{y}_{ref} \\ \dot{z} - \dot{z}_{ref} \end{bmatrix} = \begin{bmatrix} \dot{v}_x - \dot{x}_{ref} \\ \dot{v}_y - \dot{y}_{ref} \\ \dot{v}_z - \dot{z}_{ref} \end{bmatrix} \quad (17)$$

The derivation steps for STATSMC and TSMC are as follows.

3.1.1. Z-Direction Position Control

Consider the inaccuracy in mass measurement and external interference; a second-order system can be obtained as follows:

$$\begin{bmatrix} \dot{z} \\ \dot{v}_z \end{bmatrix} = \begin{bmatrix} v_z \\ a_{zd} - \frac{C_f}{m}\dot{z} + d_{m(z)} + d_z \end{bmatrix} \quad (18)$$

where d_m is the error caused by inaccuracies in quality, $-\frac{C_f}{m}\dot{z}$ is the error caused by aerodynamic drag, and d_z represents the other environmental disturbances. For the sake of convenience, let

$$D_z = -\frac{C_f}{m}\dot{z} + d_{m(z)} + d_z,$$

and (16) can be rewritten as

$$\begin{bmatrix} \dot{z} \\ \dot{v}_z \end{bmatrix} = \begin{bmatrix} v_z \\ a_{zd} + D_z \end{bmatrix} \quad (19)$$

For the z direction position control analysis, the terminal sliding-mode control (TSMC) is employed. The sliding surface (or sliding manifold) is defined to facilitate the control design. The sliding surface s_z for the z direction can be defined as

$$s_z = e_z + \frac{1}{\beta} de_z^{\frac{A}{B}} \quad (20)$$

where $\beta > 0$, positive odd integers A and B are satisfied $A > B$, and the TSMC controller can be expressed as

$$a_{zd} = -(ks_z + \beta \frac{q}{p} de_z^{2-\frac{A}{B}} + \eta \text{sgn}(s_z)) \quad (21)$$

where a_{zd} represents the desired acceleration along the z -axis, $\text{sgn}(s_z)$ denotes the sign function of the sliding surface s_z , $\eta > 0$, and condition $0 < 2 - \frac{p}{q} < 1$. In the non-singular TSMC approach, the choice of the sliding surface effectively avoids the singularity issues that are observed in traditional TSMC when $\frac{B}{A} - 1 < 0$. The Lyapunov function is defined as

$$V_z = \frac{1}{2} s_z^2 \quad (22)$$

According to (19), the time derivative of (18) is

$$\begin{aligned} \dot{s}_z &= \dot{e}_z + \frac{1}{\beta} \frac{B}{A} de_z^{\frac{A}{B}-1} \dot{e}_z \\ &= de_z + \frac{1}{\beta} \frac{B}{A} de_z^{\frac{A}{B}-1} (a_{zd} + D_z) \\ &= \frac{1}{\beta} \frac{B}{A} de_z^{\frac{A}{B}-1} (-\eta \text{sgn}(s_z) + D_z) \end{aligned} \quad (23)$$

Then, because of $\eta > D_z(max)$,

$$\dot{V}_z = s_z \dot{s}_z = \frac{1}{\beta} \frac{A}{B} de_z^{\frac{A}{B}-1} (s_z D_z - \eta |s_z|) < 0 \quad (24)$$

The Lyapunov stability of the controller is thus proven.

3.1.2. X- and Y-Direction Position Control

Below, the control law for the super-twisting algorithm terminal sliding-mode control (STATSMC) is derived and its stability is analyzed.

In the expression, the sliding-mode switching term $\eta \operatorname{sgn}(s)$ ensures that once the system state reaches the designed sliding surface, it is “attracted” to the vicinity of the sliding surface and enhances the system’s robustness against disturbances. A larger η increases the robustness of system, but it also results in greater chattering in the controller, which can adversely affect subsequent attitude control of the drone and, in severe cases, reduce the lifespan of the controller.

To mitigate undesirable chattering, the super-twisting algorithm terminal sliding-mode control (STATSMC) is introduced. The super-twisting algorithm utilizes integration to obtain the actual control input, eliminating high-frequency switching and thus avoiding chattering. It also helps to reduce the impact of external disturbances to some extent, enhancing system robustness.

Theorem 1. For the following second-order system:

$$\begin{cases} \dot{x}_1 = x_2 \\ \dot{x}_2 = f(x) + g \cdot u \end{cases} \quad (25)$$

The system is Lyapunov stable if the sliding surface satisfies the following condition:

$$\begin{cases} \dot{s} = -\lambda \sqrt{|s|} \operatorname{sgn}(s) + v \\ \dot{v} = -\alpha \operatorname{sgn}(s) \end{cases} \quad (26)$$

$\alpha, \lambda > 0$.

Proof of Theorem 1. Set the parameter in (20) as

$$\begin{cases} \dot{\lambda} = \omega_1 \sqrt{\frac{\gamma_1}{2}} \\ \alpha = \lambda \epsilon + \frac{1}{2} (\beta + 4\epsilon^2) \end{cases} \quad (27)$$

where, $\alpha, \beta, \epsilon, \lambda, \omega_1, \gamma_1 > 0$.

Let

$$\begin{bmatrix} z_1 \\ z_2 \end{bmatrix} = \begin{bmatrix} \sqrt{|s|} \operatorname{sgn}(s) \\ v \end{bmatrix} \quad (28)$$

Then, the corresponding respective derivatives are

$$\begin{cases} \dot{z}_1 = \frac{1}{2|z_1|} (-\lambda z_1 + \lambda z_2) \\ \dot{z}_2 = \dot{v} = -\alpha \operatorname{sgn}(s) = -\alpha \operatorname{sgn}(s) |s|^{\frac{1}{2}} |s|^{-\frac{1}{2}} = -\frac{\alpha}{|z_1|} z_1 \end{cases} \quad (29)$$

Let the new state variable be

$$Z = \begin{bmatrix} z_1 \\ z_2 \end{bmatrix} \quad (30)$$

Define the Lyapunov function as

$$V_0 = (\beta + 4\epsilon^2)z_1^2 + z_2^2 - 4\epsilon z_1 z_2 = Z^T P Z \quad (31)$$

where

$$P = \begin{bmatrix} \beta + 4\epsilon^2 & -2\epsilon \\ -2\epsilon & 1 \end{bmatrix} \quad (32)$$

Theorem 2. *The necessary and sufficient condition for matrix A to be positive-definite is that all eigenroots of matrix A have to be greater than zero.*

It is not hard to conclude from Theorem 2 that matrix P is positive-definite, and hence, the Lyapunov function $V_0 > 0$.

The derivative function of Equation (25) is given by

$$\begin{aligned} \dot{V}_0 &= 2(\beta + 4\epsilon^2)z_1\dot{z}_1 + 2z_2\dot{z}_2 - 4\epsilon z_2\dot{z}_1 - 4\epsilon z_1\dot{z}_2 \\ &= -\frac{1}{|Z_1|} Z^T \begin{bmatrix} -4\alpha\epsilon + \lambda(\beta + 4\epsilon^2) & -\frac{1}{2}(\beta + 4\epsilon^2) + \alpha - \lambda\epsilon \\ -\frac{1}{2}(\beta + 4\epsilon^2) + \alpha - \lambda\epsilon & 2\epsilon \end{bmatrix} Z \\ &= -\frac{1}{|z_1|} Z^T Q Z < 0. \end{aligned} \quad (33)$$

The Lyapunov stability is thus proven. \square

Similarly to (16), the position control loop model on the x-axis and y-axis of the quadrotor is a second-order system in the form of (23):

$$\begin{bmatrix} \dot{x} \\ \dot{y} \\ \dot{v}_x \\ \dot{v}_y \end{bmatrix} = \begin{bmatrix} v_x \\ v_y \\ a_{xd} - \frac{C_f}{m}\dot{x} + d_{m(x)} + d_x \\ a_{yd} - \frac{C_f}{m}\dot{y} + d_{m(y)} + d_y \end{bmatrix} \quad (34)$$

Sliding-mode surface on the x-axis and y-axis are defined as

$$\begin{bmatrix} s_x \\ s_y \end{bmatrix} = \begin{bmatrix} e_x + \frac{1}{\beta} de_x^{\frac{A}{B}} \\ e_y + \frac{1}{\beta} de_y^{\frac{A}{B}} \end{bmatrix} \quad (35)$$

And the STATSM controller is designed as

$$\begin{bmatrix} a_{xd} \\ a_{yd} \end{bmatrix} = \begin{bmatrix} -\beta \frac{B}{A} de_x^{2-\frac{A}{B}} - (K\sqrt{|s_x|} \operatorname{sgn}(s_x) + \eta \int_0^t \operatorname{sgn}(s_x) dt) \\ -\beta \frac{B}{A} de_y^{2-\frac{A}{B}} - (K\sqrt{|s_y|} \operatorname{sgn}(s_y) + \eta \int_0^t \operatorname{sgn}(s_y) dt) \end{bmatrix} \quad (36)$$

The switching term in the form of $K\sqrt{|s_x|} \operatorname{sgn}(s_x) + \eta \int_0^t \operatorname{sgn}(s_x) dt$ replaces the original $\eta \operatorname{sgn}(s)$, effectively eliminating chattering in the system. At this point,

$$\begin{bmatrix} \dot{s}_x \\ \dot{s}_y \end{bmatrix} = \begin{bmatrix} -\frac{1}{\beta} \frac{A}{B} de_x^{\frac{A}{B}-1} \sqrt{|s_x|} \operatorname{sgn}(s_x) + v_x \\ -\frac{1}{\beta} \frac{A}{B} de_y^{\frac{A}{B}-1} \sqrt{|s_y|} \operatorname{sgn}(s_y) + v_y \end{bmatrix} \quad (37)$$

$$\begin{bmatrix} \dot{v}_x \\ \dot{v}_y \end{bmatrix} = \begin{bmatrix} -\eta \operatorname{sgn}(s_x) \\ -\eta \operatorname{sgn}(s_y) \end{bmatrix} \tag{38}$$

where (35) and (36) are satisfied the form in Equation (25), and the system is Lyapunov-stable. Based on (18), thrust and the desired attitude angle can be calculated as follows:

$$\begin{cases} T = m\sqrt{a_{xd}^2 + a_{yd}^2 + (a_{zd} + g)^2} \\ \theta_{ref} = \tan^{-1}\left(\frac{\cos \psi_{ref} a_{xd} + \sin \psi_{ref} a_{yd}}{a_z + g}\right) \\ \phi_{ref} = \tan^{-1}\left(\cos \theta_{ref} \frac{\cos \psi_{ref} a_{xd} - \sin \psi_{ref} a_{yd}}{a_z + g}\right) \end{cases} \tag{39}$$

3.2. Attitude Control System

The attitude control loop of the drone is shown in Figure 4. To achieve both accuracy and responsiveness in tracking, the super-twisting algorithm terminal sliding-mode control (STABATSMC) is used to control the drone’s three attitude angles. This ensures precise tracking of the desired attitude angles and effectively suppresses chattering.

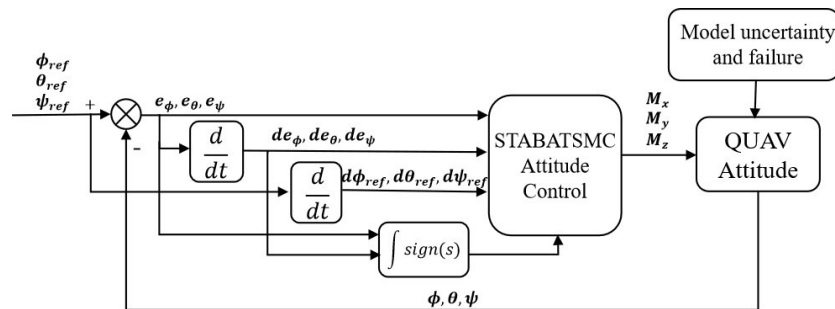


Figure 4. Attitude control loop of the quadrotor.

Considering the uncertainty of the moment of inertia of the quadrotor model, the attitude control loop can be represented by the following model:

$$\begin{bmatrix} \dot{\phi} \\ \dot{\theta} \\ \dot{\psi} \\ \dot{p} \\ \dot{q} \\ \dot{r} \end{bmatrix} = \begin{bmatrix} p \\ q \\ r \\ M_x + dJ_{xx} \\ M_y + dJ_{yy} \\ M_z + dJ_{zz} \end{bmatrix} \tag{40}$$

where dJ_{xx} , dJ_{yy} , and dJ_{zz} represent the model uncertainty disturbances due to the moment of inertia errors in the x, y, and z directions, respectively.

1. First step of designing STABATSMC:

Similar to the position control loop design, the attitude angle tracking error for the drone’s trajectory is defined as

$$\begin{bmatrix} e_\phi \\ e_\theta \\ e_\psi \end{bmatrix} = \begin{bmatrix} \phi - \phi_{ref} \\ \theta - \theta_{ref} \\ \psi - \psi_{ref} \end{bmatrix} \tag{41}$$

where ϕ , θ , and ψ represent the desired pitch, yaw, and roll angles of the drone, respectively. By differentiating the expression, we obtain

$$\begin{bmatrix} de_\phi \\ de_\theta \\ de_\psi \end{bmatrix} = \begin{bmatrix} \dot{\phi} - \dot{\phi}_{ref} \\ \dot{\theta} - \dot{\theta}_{ref} \\ \dot{\psi} - \dot{\psi}_{ref} \end{bmatrix} \approx \begin{bmatrix} p - \dot{\phi}_{ref} \\ q - \dot{\theta}_{ref} \\ r - \dot{\psi}_{ref} \end{bmatrix} \quad (42)$$

The Lyapunov function is defined as follows:

$$\begin{bmatrix} L1_\phi \\ L1_\theta \\ L1_\psi \end{bmatrix} = \frac{1}{2} \begin{bmatrix} e_\phi^2 \\ e_\theta^2 \\ e_\psi^2 \end{bmatrix} \quad (43)$$

The time derivative of (43) is

$$\begin{bmatrix} \dot{L}1_\phi \\ \dot{L}1_\theta \\ \dot{L}1_\psi \end{bmatrix} = \begin{bmatrix} \dot{e}_\phi e_\phi \\ \dot{e}_\theta e_\theta \\ \dot{e}_\psi e_\psi \end{bmatrix} \quad (44)$$

Design the virtual input as

$$\begin{bmatrix} v_\phi \\ v_\theta \\ v_\psi \end{bmatrix} = \begin{bmatrix} s_\phi + \dot{\phi}_{ref} - K_1 e_\phi \\ s_\theta + \dot{\theta}_{ref} - K_1 e_\theta \\ s_\psi + \dot{\psi}_{ref} - K_1 e_\psi \end{bmatrix} \quad (45)$$

2. Second step of designing STABATSMC:

Design the sliding-mode surface as

$$\begin{bmatrix} s_\phi \\ s_\theta \\ s_\psi \end{bmatrix} = \begin{bmatrix} e_\phi + \int_0^t \frac{1}{\beta} de_\phi^{\frac{A}{B}} d\tau \\ e_\theta + \int_0^t \frac{1}{\beta} de_\theta^{\frac{A}{B}} d\tau \\ e_\psi + \int_0^t \frac{1}{\beta} de_\psi^{\frac{A}{B}} d\tau \end{bmatrix} \quad (46)$$

To ensure the system stability, the following Lyapunov function is defined as

$$\begin{bmatrix} L2_\phi \\ L2_\theta \\ L2_\psi \end{bmatrix} = \begin{bmatrix} L1_\phi \\ L1_\theta \\ L1_\psi \end{bmatrix} + \frac{1}{2} \begin{bmatrix} s_\phi^2 \\ s_\theta^2 \\ s_\psi^2 \end{bmatrix} \quad (47)$$

The time derivative of (47) is

$$\begin{bmatrix} \dot{L}2_\phi \\ \dot{L}2_\theta \\ \dot{L}2_\psi \end{bmatrix} = \begin{bmatrix} \dot{L}1_\phi \\ \dot{L}1_\theta \\ \dot{L}1_\psi \end{bmatrix} + \begin{bmatrix} \dot{s}_\phi s_\phi \\ \dot{s}_\theta s_\theta \\ \dot{s}_\psi s_\psi \end{bmatrix} \quad (48)$$

Substituting (45) into (48),

$$\begin{bmatrix} \dot{L}2_\phi \\ \dot{L}2_\theta \\ \dot{L}2_\psi \end{bmatrix} = \begin{bmatrix} -\dot{e}_\phi e_\phi + (\dot{s}_\phi + e_\phi) s_\phi \\ -\dot{e}_\theta e_\theta + (\dot{s}_\theta + e_\theta) s_\theta \\ -\dot{e}_\psi e_\psi + (\dot{s}_\psi + e_\psi) s_\psi \end{bmatrix} \quad (49)$$

In order to ensure system stability, (49) should require the following condition:

$$\begin{bmatrix} (\dot{s}_\phi + e_\phi)s_\phi \\ (\dot{s}_\theta + e_\theta)s_\theta \\ (\dot{s}_\psi + e_\psi)s_\psi \end{bmatrix} \leq 0 \tag{50}$$

Denote the torques that the quadrotor needs to generate in x, y, and z directions as M_x , M_y , and M_z , respectively. Then, design the controller as

$$\begin{bmatrix} M_x \\ M_y \\ M_z \end{bmatrix} = \begin{bmatrix} -J_{xx}(qr \frac{J_{zz}-J_{yy}}{J_{xx}} \beta \frac{B}{A} de_\phi^{2-\frac{A}{B}} + cp^2 + (K\sqrt{|s_\phi|}sgn(s_\phi) + \tilde{\eta} \int_0^t sgn(s_\phi)dt) + \dot{\phi}_{ref}) \\ -J_{yy}(pr \frac{J_{xx}-J_{zz}}{J_{yy}} \beta \frac{B}{A} de_\theta^{2-\frac{A}{B}} + cq^2 + (K\sqrt{|s_\theta|}sgn(s_\theta) + \tilde{\eta} \int_0^t sgn(s_\theta)dt) + \dot{\theta}_{ref}) \\ -J_{zz}(pq \frac{J_{yy}-J_{xx}}{J_{zz}} \beta \frac{B}{A} de_\psi^{2-\frac{A}{B}} + cr^2 + (K\sqrt{|s_\psi|}sgn(s_\psi) + \tilde{\eta} \int_0^t sgn(s_\psi)dt) + \dot{\psi}_{ref}) \end{bmatrix} \tag{51}$$

At this point,

$$\begin{bmatrix} \dot{s}_\phi \\ \dot{s}_\theta \\ \dot{s}_\psi \end{bmatrix} = \begin{bmatrix} -\frac{1}{\beta} \frac{A}{B} de_x^{\frac{A}{B}-1} \sqrt{|s_\phi|}sgn(s_\phi) + v_\phi \\ -\frac{1}{\beta} \frac{A}{B} de_y^{\frac{A}{B}-1} \sqrt{|s_\theta|}sgn(s_\theta) + v_\theta \\ -\frac{1}{\beta} \frac{A}{B} de_x^{\frac{A}{B}-1} \sqrt{|s_\psi|}sgn(s_\psi) + v_\psi \end{bmatrix} \tag{52}$$

$$\begin{bmatrix} \dot{v}_\phi \\ \dot{v}_\theta \\ \dot{v}_\psi \end{bmatrix} = \begin{bmatrix} -\tilde{\eta}sgn(s_\phi) \\ -\tilde{\eta}sgn(s_\theta) \\ -\tilde{\eta}sgn(s_\psi) \end{bmatrix} \tag{53}$$

Clearly, (52) and (53) conform to the form of (24). Lyapunov stability of the attitude controller is proved.

3. Third step of designing STABATSMC:

To further enhance the robustness of the system, the parameter η in Equation (51) is reformulated through an adaptive law as follows:

$$\tilde{\eta} = \eta_0 + \int_0^t d\eta \tag{54}$$

$$d\eta = \begin{cases} \beta_0 & , \eta \leq \delta_0, \\ a|s|sgn(|s| - \delta_0) & , \eta > \delta_0. \end{cases} \tag{55}$$

β_0 and δ_0 should requires $\beta_0, \delta_0 > 0$.

By the control allocation matrix, the rotor speed of the quadrotor can be obtained as

$$\begin{bmatrix} \omega_1^2 \\ \omega_2^2 \\ \omega_3^2 \\ \omega_4^2 \end{bmatrix} = M_c^{-1} \cdot \begin{bmatrix} T \\ M_x \\ M_y \\ M_z \end{bmatrix} \tag{56}$$

$$M_c = \begin{bmatrix} C_T & C_T & C_T & C_T \\ 0 & dC_T & 0 & -dC_T \\ -dC_T & 0 & dC_T & 0 \\ C_M & -C_M & C_M & -C_M \end{bmatrix} \tag{57}$$

where M_c denotes the control allocation matrix of the quadrotor.

4. Simulation Result and Analysis

In this section, the efficiency of the proposed controller is validated through simulation experiments. In the simulations, the initial position and initial attitude of the quadrotor are

set to $[0; 0; 0]$ m and $[0; 0; 0]$ rad, respectively. The quadrotor model parameters adopted in the experiment refer to the parameters mentioned in Sun et al.'s work [40]. The static parameters and control parameters of the quadrotor are shown in Tables 1 and 2, respectively.

The AIBS-ABFNITSMC system designed by Jiao et al. in [7] showed good performance in dealing with external disturbances, but the case of sudden failure in quadrotor flight was not considered. Backstepping control can moderate the control output; backstepping terminal sliding-mode control (BTSMC) is the control method with high robustness. In this section, external disturbances, model uncertainties, and sudden rotor faults are considered to demonstrate the superiority of the designed controller compared with TSMC, BTSMC, and AIBS-ABFNITSMC.

Table 1. Physical parameters of the quadrotor.

Parameter	Value	Meaning
m	0.41	the mass of the quadrotor
g	9.78	acceleration of gravity
d	0.145	the arm length of the quadrotor
J_{xx}	1.45×10^{-3}	moment of inertia on the x-axis
J_{yy}	1.45×10^{-3}	moment of inertia on the y-axis
J_{zz}	2.52×10^{-3}	moment of inertia on the z-axis
C_T	1.90×10^{-6}	lift coefficient of the quadrotor
C_M	1.50×10^{-3}	moment coefficient of the quadrotor
C_f	5.60×10^{-4}	aerodynamic drag of the quadrotor during flight

Table 2. Control parameters of the quadrotor.

Controller Name	Control Parameter	Parameter Value
Position control on x and y axis	A	7
	B	5
	β	0.5
	K	1
	η	1
Position control on z-axis	A	5
	B	3
	β	0.05
	K	100
	η	150
Attitude control	A	7
	B	5
	β	0.05
	K	5
	η_0	5
	a	3
	c	0.01
	β_0	3
δ_0	2	

The proposed control scheme was compared with control loops based on backstepping terminal sliding-mode control and terminal sliding-mode control. The experiments considered the following disturbances: external environmental interference, errors caused by model inaccuracies, and rotor looseness faults.

Assume that during the flight, it is subjected to environmental disturbances in the x and y directions that follow a sinusoidal function. Due to model uncertainty, the quadrotor's mass is affected; additionally, when $t > 40$ s, a rotor looseness fault occurs, leading to a

decrease in rotor efficiency. The mathematical models for these three disturbances and faults are presented in Table 3, Table 4 and Table 5, respectively.

Table 3. External interference of the quadrotor.

External Interference Parameter	Value	Meaning
D_x	$0.1\sin(2t)$	interference in the x direction
D_y	$0.2\sin(2t)$	interference in the y direction
D_z	0	interference in the z direction

Table 4. Model uncertainty of the quadrotor.

Model Uncertainty Parameter	Value	Meaning
Δm	2.650×10^{-2}	error of the mass of the quadrotor
ΔJ_{xx}	8.725×10^{-5}	error of the moment of inertia on the x-axis
ΔJ_{yy}	-8.725×10^{-5}	error of the moment of inertia on the y-axis
ΔJ_{zz}	0	error of the moment of inertia on the z-axis

Table 5. Rotor speed drop fault of the quadrotor.

Speed Drop Parameter	Value
$\Delta \tilde{\omega}_1$	$-(100\sin(t) + 100)$
$\Delta \tilde{\omega}_2$	-100
$\Delta \tilde{\omega}_3$	$-200\sin(0.5t)$
$\Delta \tilde{\omega}_4$	0

4.1. Case 0

The trajectory tracking of a quadrotor without fault is considered. The trajectory curve followed is the same as in Case 1. Figure 5 shows the three-dimensional trajectory diagram of the different control schemes and visually compares their tracking performance. In order to provide a more comprehensive performance evaluation, x, y and z directions tracking trajectories and Euler angle response curves of the quadrotor are plotted. Figures 6 and 7 show the simulation results.

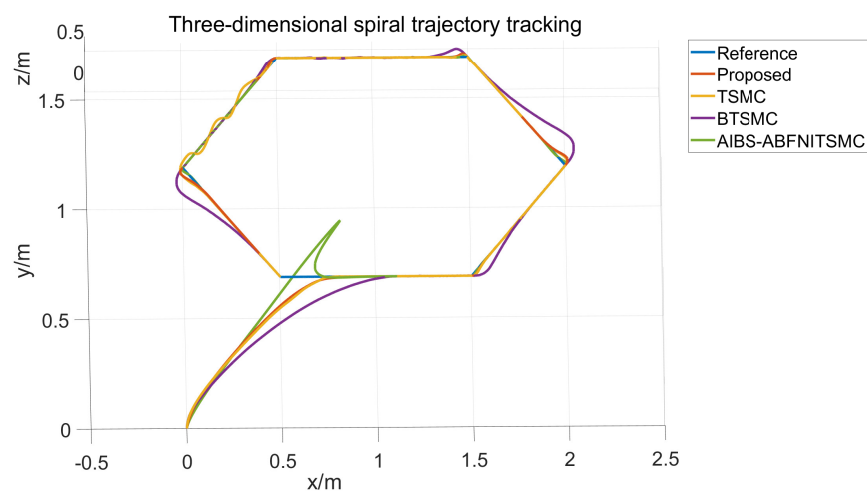


Figure 5. The three-dimensional hexagon trajectory tracking of quadrotor without fault.

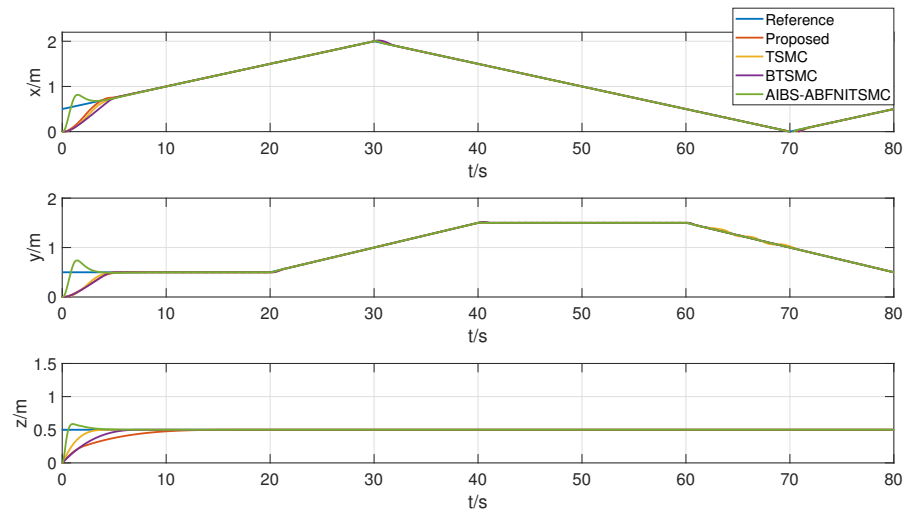


Figure 6. Displacement motion in hexagonal trajectory tracking (no faults).

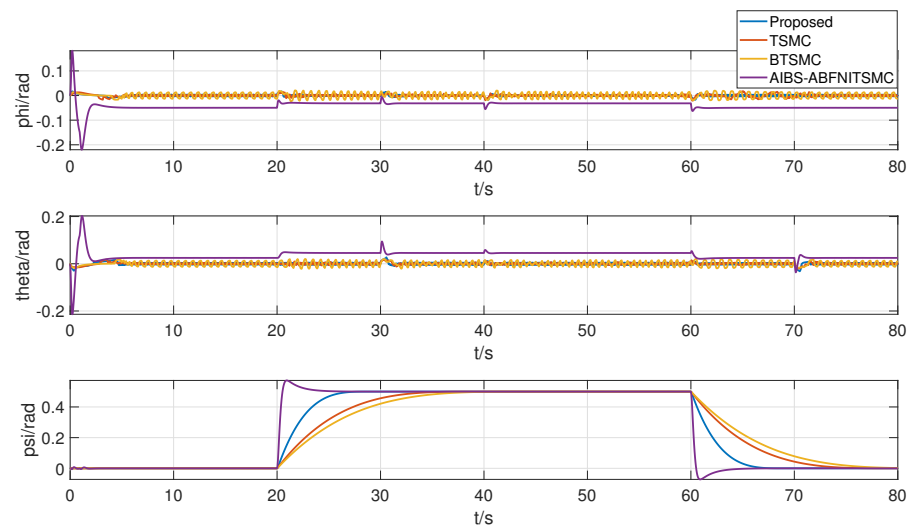


Figure 7. Rotational motion in hexagonal trajectory tracking (no faults).

All these control methods can achieve effective fault-free control of the quadrotor and accurate tracking of the desired trajectory. The selected controller has good trajectory tracking performance. However, we find that the attitude angle responses of TSMC and BTSMC exist chattering vibration. Note that severe chattering has some impact on the actuator and control performance.

4.2. Case 1

In this case, the drone's task is to track the desired hexagon trajectory by taking into account the aforementioned disturbances and failures. Figure 8 shows the three-dimensional trajectory diagram of the two control schemes, and intuitively compares the tracking performance of the two control schemes. To provide a more comprehensive performance evaluation, error curves for x , y , z directions and Euler angles of the quadrotor are plotted. Figures 8–12 show the simulation results.

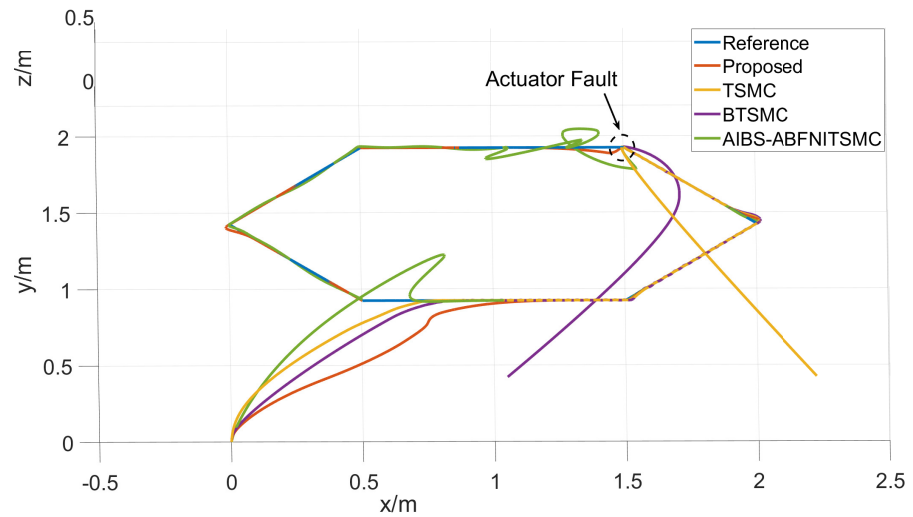


Figure 8. The three-dimensional hexagon trajectory tracking of the quadrotor.

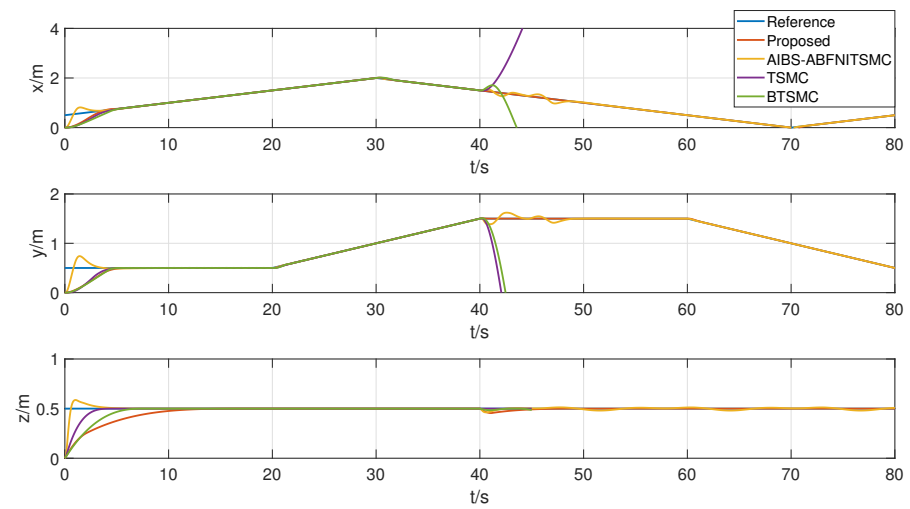


Figure 9. Displacement motion in hexagonal trajectory tracking.

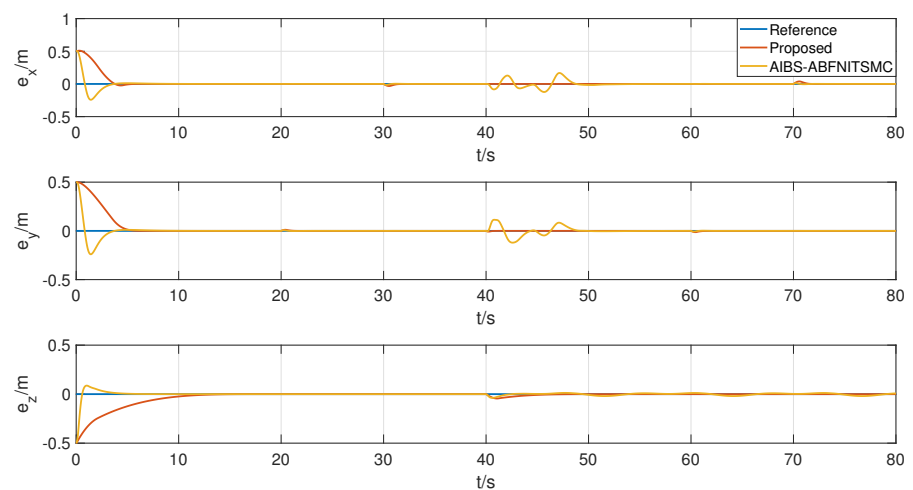


Figure 10. Displacement motion error in hexagonal trajectory tracking.

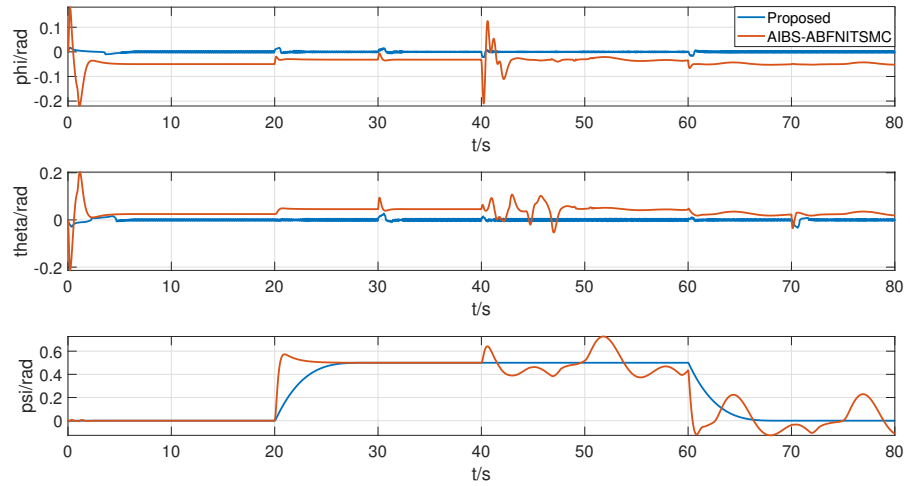


Figure 11. Rotational motion in hexagonal trajectory tracking.

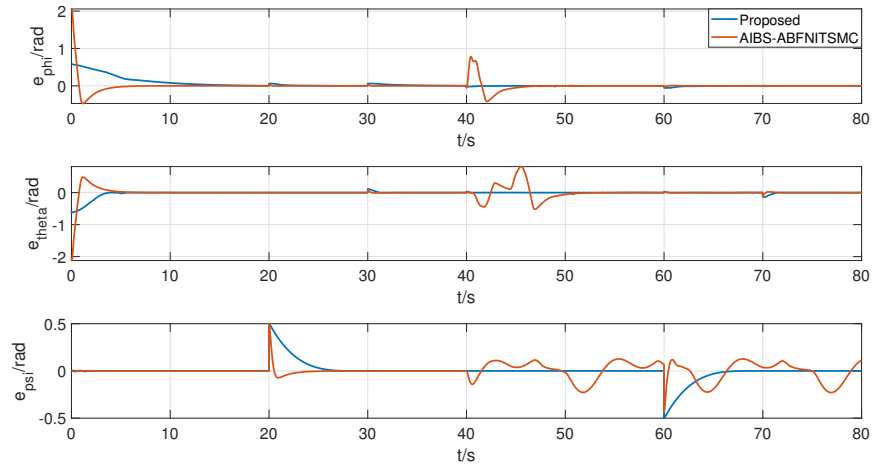


Figure 12. Rotational motion error in hexagonal trajectory tracking.

The trajectory to be tracked by the UAV is defined as follows:

$$x_{ref} = \begin{cases} 0.5 + 0.05t & 0 \leq t < 30 \\ 2 - 0.05t & 30 \leq t < 70 \\ 0.05t & 70 \leq t \leq 80 \end{cases} \quad (58)$$

$$y_{ref} = \begin{cases} 0.5 & 0 \leq t < 20 \\ 0.5 + 0.05t & 20 \leq t < 40 \\ 1.5 & 40 \leq t < 60 \\ 1.5 - 0.05t & 60 \leq t \leq 80 \end{cases} \quad (59)$$

$$z_{ref} = -0.5 \quad (60)$$

$$\psi_{ref} = \begin{cases} 0 & 0 \leq t < 20 \\ 0.5 & 20 \leq t < 60 \\ 0 & 60 \leq t \leq 80 \end{cases} \quad (61)$$

Due to the initial position and attitude being set to zero, the quadrotor attempts to quickly converge to the desired trajectory, resulting in excessive roll and pitch angles during the initial phase of the simulation, which causes significant tracking errors.

In Figures 8–12, the proposed controller can track the desired trajectory in a limited time under multiple disturbances and faults, showing better performance. Compared with other controllers, STATSMC-STABATSMC can suppress buffeting effectively. In addition, the designed controller can track the desired trajectory accurately. When $t > 40$ s, STATSMC-STABATSMC can track the trajectory and stabilize the attitude response in a certain range under actuator faults.

According to Figures 8 and 9, these controllers can cope with the faults caused by external interference and model uncertainty. But BTSMC and TSMC cannot process the sudden actuator faults. When the rotor fails, the quadrotor will crash. TSMC exhibits high sensitivity to error changes, with an exponential relationship between the control output and the error change de . This property guarantees that the error e converges to 0 within a finite time, ensuring the robustness of the system. However, in the case of severe sudden failures such as rotor failure, drastic changes in error can lead to controller saturation, manifesting as output oscillation, which reduces controller performance and may even accelerate its failure.

Moderating the control output and suppressing chattering are effective strategies to address the aforementioned issues. Backstepping control simplifies nonlinear systems and mitigates SMC buffeting effectively, but BTSMC cannot handle actuator faults in Figures 8 and 9. In TSMC, the switching term $\eta \operatorname{sgn}(s)$ ensures controller robustness, but a larger η value exacerbates buffeting, shortening controller lifespan and potentially causing quadrotor crashes. To resolve this contradiction, we introduce the super-twisting algorithm on top of BTSMC, adjusting η through adaptive laws. This ensures system performance while suppressing buffeting, thereby solving the problems. Notably, both TSMC and BTSMC lose control when $t > 40$ s, failing to track the desired trajectory. Figures 10–12 present separate analyses of STATSMC-STABATSMC and AIBS-ABFNITSMC.

Compared to AIBS-ABFNITSMC, the proposed controller demonstrates superior performance in handling rotor failures and rapidly restores accurate tracking of the preset trajectory. As illustrated in Figures 11 and 12, the pitch and roll angles of AIBS-ABFNITSMC fail to converge to 0. The attitude angles, particularly the yaw angle, exhibit significant oscillation after $t > 40$ s. This oscillation stems from the unbalanced starting torque among the rotors. In contrast, the designed controller, when faced with failures and disturbances, avoids such issues. Attitude angles remain stable, with no buffeting, exhibiting superior performance.

By comparison, it is evident that the proposed controller outperforms similar controllers. The hexagonal trajectory is relatively straightforward. To further demonstrate the superiority of the proposed controller, we will compare the performance of AIBS-ABFNITSMC and STATSMC-STABATSMC in Case 2 using more complex trajectories.

4.3. Case 2

The tracking performance of the quadrotor UAV under a disturbed environment for complex trajectories is evaluated. Simulation results are presented in Figures 13–17.

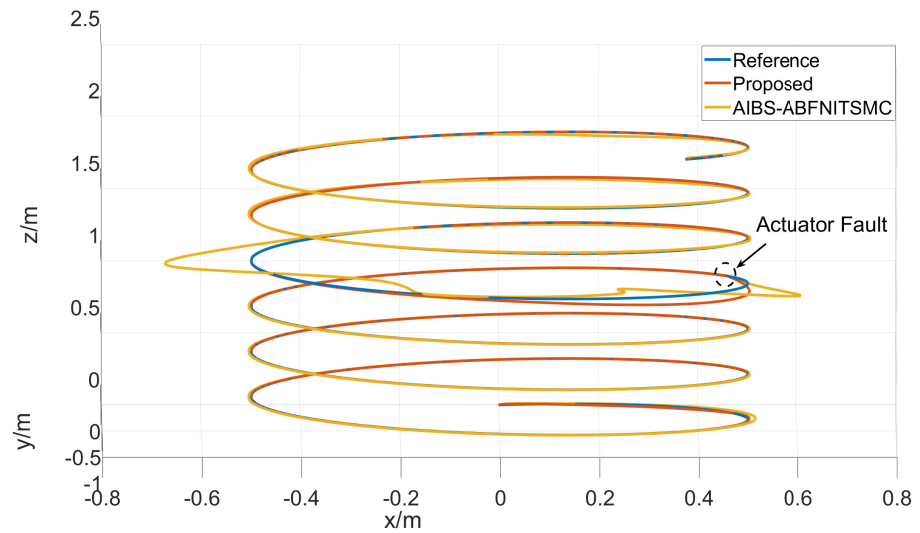


Figure 13. The three-dimensional spiral trajectory tracking of the quadrotor.

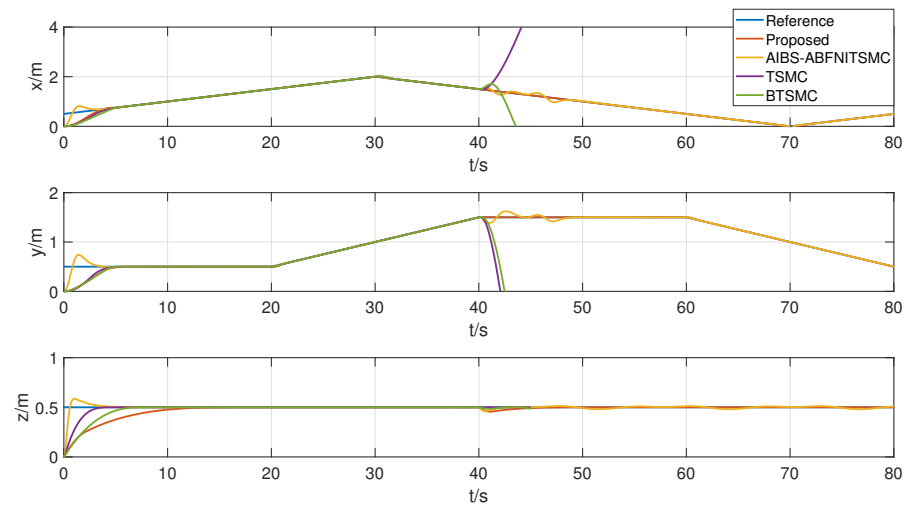


Figure 14. Displacement motion in spiral trajectory tracking.

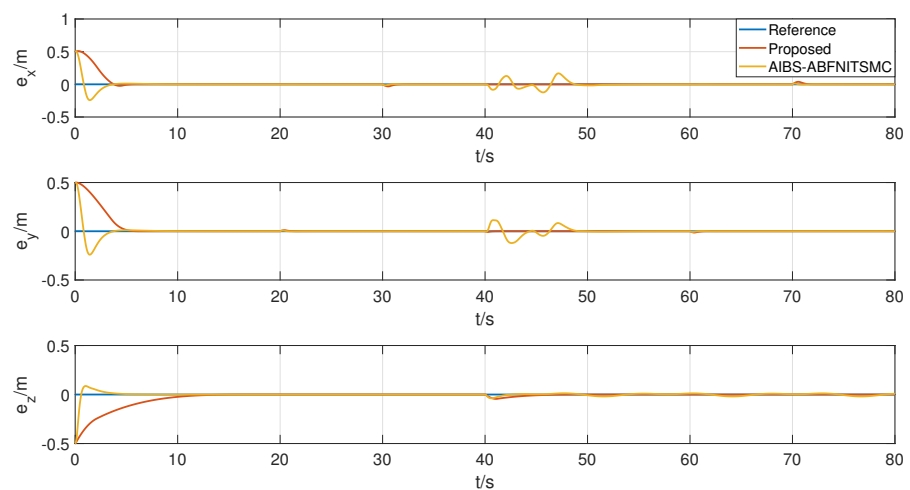


Figure 15. Displacement motion error in spiral trajectory tracking.

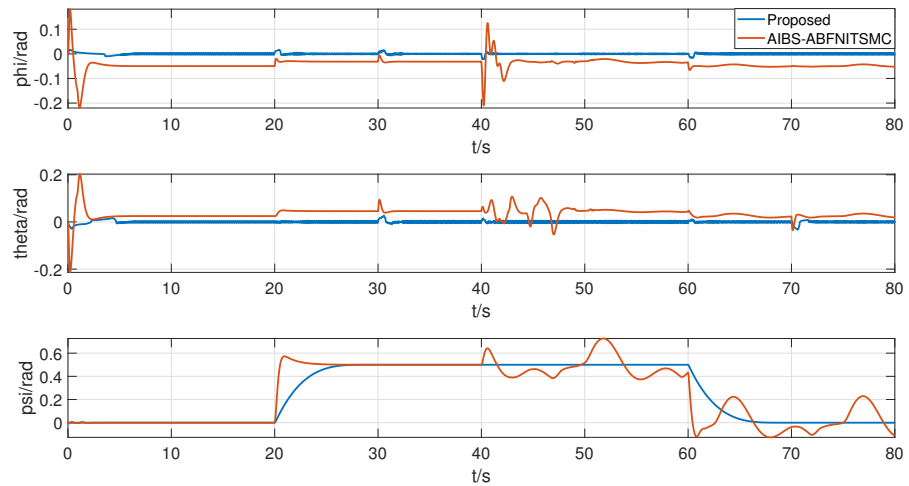


Figure 16. Rotational motion in spiral trajectory tracking.

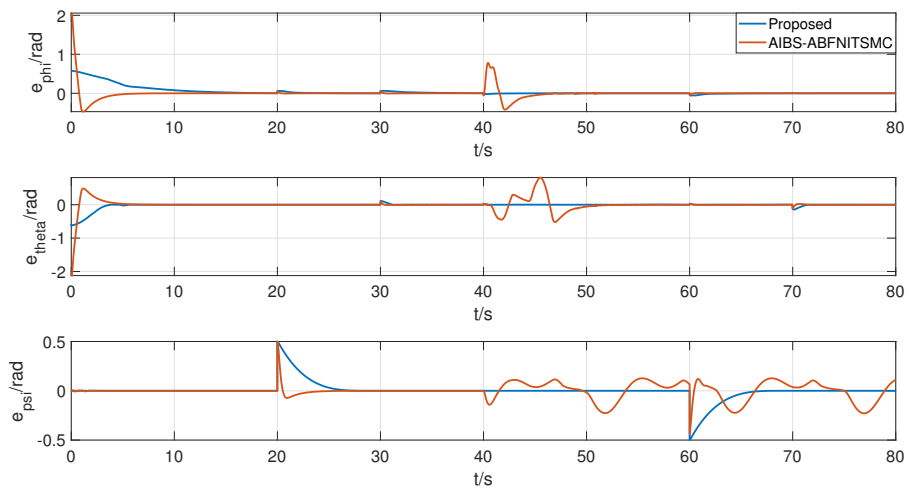


Figure 17. Rotational motion error in spiral trajectory tracking.

The desired trajectory is defined as follows:

$$x_{\text{ref}} = 0.5\sin(0.5t) \tag{62}$$

$$y_{\text{ref}} = 0.5\cos(0.5t) - 0.5 \tag{63}$$

$$z_{\text{ref}} = -0.025t \tag{64}$$

$$\psi_{\text{ref}} = \begin{cases} 0 & 0 \leq t < 20 \\ 0.5 & 20 \leq t < 60 \\ 0 & 60 \leq t \leq 80 \end{cases} \tag{65}$$

As shown in Figures 13 and 14, the tracking performance of AIBS-ABFNITSMC is inferior to that of the proposed controller, requiring a longer recovery time in response to actuator failures. Figure 13 depicts the attitude angle tracking of the pitch, yaw, and roll channels during quadrotor flight. Due to the torque imbalance caused by the fault, the quadrotor experiences significant jitter, making accurate yaw angle tracking unachievable. In contrast, the proposed controller tracks the desired trajectory and attitude more rapidly and accurately, proving its robustness and superiority.

4.4. Case 3

The tracking performance of the quadrotor UAV under a measurement noise environment for complex trajectories is evaluated. Simulation results are presented in Figures 18–21.

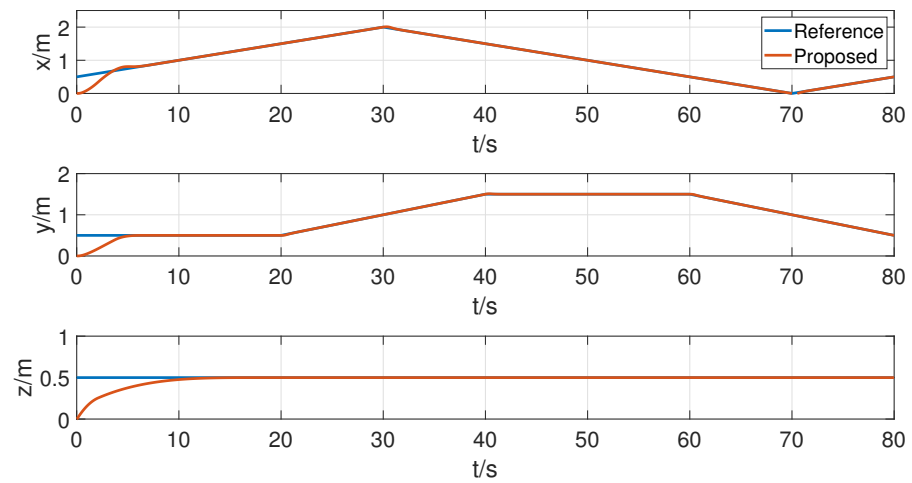


Figure 18. Displacement motion in rectangle trajectory tracking.

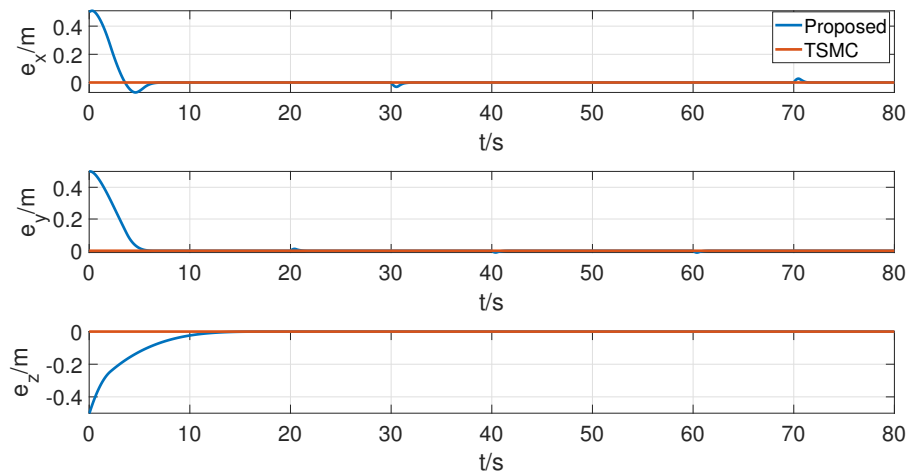


Figure 19. Displacement motion error in rectangle trajectory tracking.

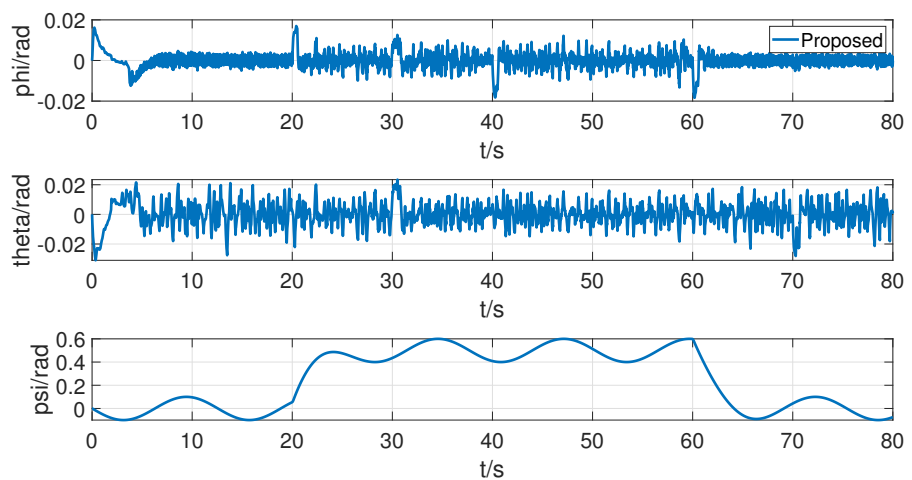


Figure 20. Rotational motion in rectangle trajectory tracking.

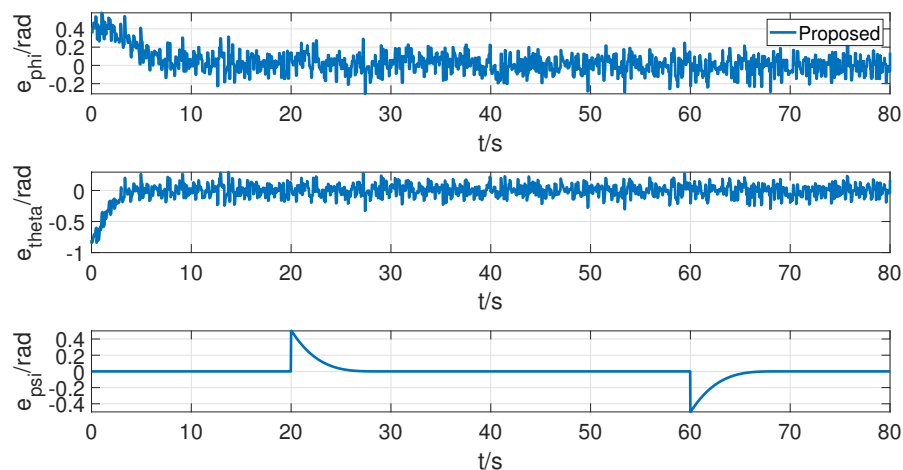


Figure 21. Rotational motion error in rectangle trajectory tracking.

The desired trajectory is the same as in Case 1, and the measurement noise exists in the attitude angle observer of the quadrotor controller. The observers for pitch and roll channels have Gaussian noise with a mean of 0.1 and a variance of 0.01. A sinusoidal disturbance with an amplitude of 0.1 exists in the yaw channel.

As shown in Figures 18 and 19, the proposed controller can accurately track trajectories in an environment with measurement noise. Figure 20 depicts the attitude angle tracking of the pitch, yaw, and roll channels during quadrotor flight. Due to the presence of noise, there is a certain degree of chattering in the pitch and roll channels, but the oscillation angles are small and do not affect the flight mission. The yaw channel exhibits larger fluctuations; however, in Figure 21, the tracking error of the yaw angle can converge to 0. This is due to the impact of measurement noise on the calculation of the desired attitude angle in the controller. To address this issue, a robust observer will be designed in the future to reduce the impact of measurement noise.

5. Conclusions and Future Research

In this paper, a dynamic model of a quadrotor vehicle is established by means of a Newton–Euler equation, which takes into account the uncertainty of parameters, external interference factors, and actuator sudden failure. A STATSMC scheme for position loop is proposed, which derives the desired attitude based on the desired position decoupling equation. In addition, a new STABATSMC attitude tracking control method is proposed, which combines terminal sliding-mode control with backstepping control, adaptive estimation and super-twisting algorithm. The accuracy decrease caused by buffeting and control output saturation in TSMC is effectively improved. In order to reduce buffeting, the saturation function is adopted. The stability of the control system is verified by using Lyapunov stability theory. Finally, the comparison and analysis with AIBS-ABFNITSM show that the designed control scheme has better performance and robustness against external random interference.

Future research will involve validating the performance of the STATSMC-STABATSMC control scheme using a real quadrotor in trajectory tracking tasks. We are building a physical simulation platform, and the results in the paper will be further verified by experiments in the future. Given the inherent limitations of Euler angles, further exploration of quaternion applications in quadrotor attitude trajectory tracking control is also warranted. In addition, considering that the effect of the existing controller in the face of measurement faults is not ideal, this problem will be solved by adding a robust observer in our future work.

Author Contributions: Conceptualization, Y.F. and Y.Z.; methodology, Y.F.; software, Y.F.; validation, Y.F., Y.Z. and Z.H.; formal analysis, Y.F.; investigation, J.W.; resources, Y.Z.; data curation, Y.Z.; writing—original draft preparation, Y.F.; writing—review and editing, Y.Z.; visualization, Y.F.; supervision, Z.H.; project administration, Z.H.; funding acquisition, Y.Z. All authors have read and agreed to the published version of the manuscript.

Funding: National Natural Science Foundation of China, Grant/Award Number: 52202502; Aeronautical Science Fund, Grant/Award Number: 20230001053006.

Data Availability Statement: The data are contained within the article.

Conflicts of Interest: The authors declare no conflicts of interest.

References

1. Wang, D.; Pan, Q.; Shi, Y.; Hu, J.; Zhao, C. Efficient nonlinear model predictive control for quadrotor trajectory tracking: Algorithms and experiment. *IEEE Trans. Cybern.* **2021**, *51*, 5057–5068. [[CrossRef](#)] [[PubMed](#)]
2. Zhang, K.; Shi, Y.; Sheng, H. Robust nonlinear model predictive control based visual servoing of quadrotor UAVs. *IEEE/ASME Trans. Mechatron.* **2021**, *26*, 700–708. [[CrossRef](#)]
3. Tang, L.; Wang, H.; Liu, Z.; Wang, Y. A real-time quadrotor trajectory planning framework based on b-spline and nonuniform kinodynamic search. *J. Field Robot.* **2021**, *38*, 452–475. [[CrossRef](#)]
4. Chen, M.; Xiong, S.; Wu, Q. Tracking flight control of quadrotor based on disturbance observer. *IEEE Trans. Syst. Man Cybern. Syst.* **2021**, *51*, 1414–1423. [[CrossRef](#)]
5. Tran, T.-T.; Ge, S.S.; He, W. Adaptive control of a quadrotor aerial vehicle with input constraints and uncertain parameters. *Int. J. Control* **2018**, *91*, 1140–1160. [[CrossRef](#)]
6. Song, Y.; Liu, X.; Xu, B.; Zhang, Y.; Yang, C. Disturbance observer-based control of quadrotors with motor response delay and throttle nonlinearity. In Proceedings of the 2020 International Conference on Unmanned Aircraft Systems (ICUAS), Athens, Greece, 1–4 September 2020; pp. 182–187.
7. Li, Z.; Zhang, B. Application Study of UAV and IOT Technology in Intelligent Detection of Bridge Engineering. In Proceedings of the 2022 International Conference on Machine Learning, Cloud Computing and Intelligent Mining (MLCCIM), Xiamen, China, 5–7 August 2022; pp. 13–18.
8. Afonso, B.; Liu, H. Wireless Sensing for Structural Health Monitoring of Bridges by Unmanned Aerial Vehicle (UAV) via BLE Communication. In Proceedings of the 2024 International Wireless Communications and Mobile Computing (IWCMC), Ayia Napa, Cyprus, 27–31 May 2024; pp. 1674–1678.
9. Sun, S.; Franchi, A. Nonlinear MPC for Full-Pose Manipulation of a Cable-Suspended Load using Multiple UAVs. In Proceedings of the 2023 International Conference on Unmanned Aircraft Systems (ICUAS), Warsaw, Poland, 6–9 June 2023; pp. 969–975.
10. Li, B.; Gong, W.; Yang, Y.; Xiao, B.; Ran, D. Appointed fixed time observer-based sliding mode control for a quadrotor UAV under external disturbances. *IEEE Trans. Aerosp. Electron. Syst.* **2021**, *58*, 290–303. [[CrossRef](#)]
11. Pan, J.; Shao, B.; Xiong, J.; Zhang, Q. Attitude control of quadrotor UAVs based on adaptive sliding mode. *Int. J. Control Autom. Syst.* **2023**, *21*, 2698–2707. [[CrossRef](#)]
12. Pouzesh, M.; Mobayen, S. Event-triggered fractional-order sliding mode control technique for stabilization of disturbed quadrotor unmanned aerial vehicles. *Aerosp. Sci. Technol.* **2022**, *121*, 107337. [[CrossRef](#)]
13. Sonugür, G. A Review of quadrotor UAV: Control and SLAM methodologies ranging from conventional to innovative approaches. *Robot. Auton. Syst.* **2023**, *161*, 104342. [[CrossRef](#)]
14. Xiong, J.; Pan, J.; Chen, G.; Zhang, X.; Ding, F. Sliding mode dual-channel disturbance rejection attitude control for a quadrotor. *IEEE Trans. Ind. Electron.* **2021**, *69*, 10489–10499. [[CrossRef](#)]
15. Labbadi, M.; Cherkaoui, M. Robust adaptive nonsingular fast terminal sliding-mode tracking control for an uncertain quadrotor UAV subjected to disturbances. *ISA Trans.* **2020**, *99*, 290–304. [[CrossRef](#)]
16. Rojsiraphisal, T.; Mobayen, S.; Asad, J.H.; Vu, M.T.; Chang, A.; Puangmalai, J. Fast terminal sliding control of underactuated robotic systems based on disturbance observer with experimental validation. *Mathematics* **2021**, *9*, 1935. [[CrossRef](#)]
17. Lim, D.; Kim, H.; Yee, K. Uncertainty propagation in flight performance of multirotor with parametric and model uncertainties. *Aerosp. Sci. Technol.* **2022**, *122*, 107398. [[CrossRef](#)]
18. Kim, H.; Ahn, H.; Chung, Y.; You, K. Quadrotor Position and Attitude Tracking Using Advanced Second-Order Sliding Mode Control for Disturbance. *Mathematics* **2023**, *11*, 4786. [[CrossRef](#)]
19. Song, W.; Sun, L.; Wang, Q. Nonlinear Constrained Optimization Method for Dynamic Conversion Corridor of Tilt-Rotor Aircraft. *J. Guid. Control. Dyn.* **2024**, *47*, 2661–2666. [[CrossRef](#)]

20. Jiao, J.; Sun, L.; Tan, W.; Liu, X.; Shang, Z. Adaptive Flying Assistance Controller Design to Suppress Nonlinear Pilot-Induced Oscillations. *J. Guid. Control. Dyn.* **2024**, *47*, 2133–2147. [[CrossRef](#)]
21. Jiao, J.; Sun, L.; Tan, W.; Xu, S.; Liu, X. Identifying Pilot Control Adaptations to Sudden Changes in Aircraft Dynamics. *J. Guid. Control. Dyn.* **2023**, *46*, 1408–1415. [[CrossRef](#)]
22. Barghandan, S.; Badamchizadeh, A.M.; Jahed-Motlagh, M.R.J. Improved adaptive fuzzy sliding mode controller for robust fault tolerant of a Quadrotor. *Int. J. Control Autom. Syst.* **2017**, *15*, 427–441. [[CrossRef](#)]
23. Guo, K.; Jia, J.; Yu, X.; Guo, L.; Xie, L. Multiple observers based anti-disturbance control for a quadrotor UAV against payload and wind disturbances. *Control Eng. Pract.* **2020**, *102*, 104560 [[CrossRef](#)]
24. Mofid, O.; Mobayen, S. Adaptive Finite-Time Backstepping Global Sliding Mode Tracker of Quad-Rotor UAVs Under Model Uncertainty, Wind Perturbation, and Input Saturation. *IEEE Trans. Aerosp. Electron. Syst.* **2022**, *58*, 140–151. [[CrossRef](#)]
25. Sini, S.; Ananthan, T. A Disturbance Observer Based Control for Quadrotor Aircraft Subject to Wind Gusts. In Proceedings of the 2022 IEEE International Conference on Signal Processing, Informatics, Communication and Energy Systems (SPICES), Thiruvananthapuram, India, 10–12 March 2022; pp. 491–496.
26. Zhao, K.; Zhang, J.; Ma, D.; Xia, Y. Composite disturbance rejection attitude control for quadrotor with unknown disturbance. *IEEE Trans. Ind. Electron.* **2019**, *67*, 6894–6903. [[CrossRef](#)]
27. Choi, Y.-C.; Ahn, H.-S. Nonlinear robust control of a quadrotor for point tracking based on nonlinear disturbance observer. In Proceedings of the 2015 15th International Conference on Control, Automation and Systems (ICCAS), Busan, Republic of Korea, 13–16 October 2015; pp. 286–289.
28. Yu, S.; Yu, X.; Shirinzadeh, B.; Man, Z. Continuous finite-time control for robotic manipulators with terminal sliding mode. *Automatica* **2005**, *41*, 1957–1964. [[CrossRef](#)]
29. Shao, K.; Zheng, J.; Huang, K.; Wang, H.; Man, Z.; Fu, M. Finite-time control of a linear motor positioner using adaptive recursive terminal sliding mode. *IEEE Trans. Ind. Electron.* **2019**, *67*, 6659–6668. [[CrossRef](#)]
30. Cui, R.; Chen, L.; Yang, C.; Chen, M. Extended state observer-based integral sliding mode control for an underwater robot with unknown disturbances and uncertain nonlinearities. *IEEE Trans. Ind. Electron.* **2017**, *64*, 6785–6795. [[CrossRef](#)]
31. Lian, S.; Meng, W.; Shao, K.; Zheng, J.; Zhu, S.; Li, H. Full Attitude Control of a Quadrotor Using Fast Nonsingular Terminal Sliding Mode with Angular Velocity Planning. *IEEE Trans. Ind. Electron.* **2022**, *70*, 3975–3984. [[CrossRef](#)]
32. Ebrahimi, N.; Ozgoli, S.; Ramezani, A. Model-free high-order terminal sliding mode controller for Lipschitz nonlinear systems. Implemented on Exoped[®] exoskeleton robot. *Int. J. Syst. Sci.* **2021**, *52*, 1061–1073. [[CrossRef](#)]
33. Mofid, O.; Mobayen, S.; Zhang, C.; Esakki, B. Desired tracking of delayed quadrotor UAV under model uncertainty and wind disturbance using adaptive super-twisting terminal sliding mode control. *ISA Trans.* **2022**, *123*, 455–471. [[CrossRef](#)]
34. Jiao, S.; Wang, J.; Hua, Y.; Zhuang, Y.; Yu, X. Trajectory-Tracking Control for Quadrotors Using an Adaptive Integral Terminal Sliding Mode under External Disturbances. *Drones* **2024**, *8*, 67. [[CrossRef](#)]
35. Kim, H.; Ahn, H.; You, K. Quadrotor Attitude Control Using Adaptive Novel Super-Twisting Algorithm. In Proceedings of the 2023 23rd International Conference on Control, Automation and Systems (ICCAS), Yeosu, Republic of Korea, 17–20 October 2023; pp. 517–521.
36. Zhang, Y.; Su, M.; Cheng, Z.; Liu, L.; Wang, B. Adaptive Super Twisting Sliding Mode Control for Flying-Wing UAV. In Proceedings of the 2021 33rd Chinese Control and Decision Conference (CCDC), Kunming, China, 22–24 May 2021; pp. 236–241.
37. Zakeri, E.; Xie, W.-F. Robust Photogrammetry-Based Online Pose Correction of Industrial Robots Employing Adaptive Integral Terminal Fractional-Order Super-Twisting Algorithm. In Proceedings of the 2022 Sixth IEEE International Conference on Robotic Computing (IRC), Naples, Italy, 5–7 December 2022; pp. 119–126.
38. Cheng, C.; Liu, Y.; Guo, X. Nonlinear Speed Control of PMSM Based on Improved Super Twisting Algorithm Considering Lumped Disturbance Compensation. In Proceedings of the 2021 IEEE 4th International Electrical and Energy Conference (CIEEC), Wuhan, China, 28–30 May 2021; pp. 1–6.
39. Huang, H.; Sun, G.; Zhang, D.; Huang, G.; Xu, X.; Zhang, B. Adaptive Attitude Control for a Kind of Heavy-Lift Launch Vehicle Based on Super-Twisting Algorithm. In Proceedings of the 2021 China Automation Congress (CAC), Beijing, China, 22–24 October 2021; pp. 3288–3293.
40. Sun, S.; Wang, X.; Chu, Q.; and C. d. Visser, Incremental Nonlinear Fault-Tolerant Control of a Quadrotor with Complete Loss of Two Opposing Rotors. *IEEE Trans. Robot.* **2021**, *37*, 116–130. [[CrossRef](#)]

Disclaimer/Publisher’s Note: The statements, opinions and data contained in all publications are solely those of the individual author(s) and contributor(s) and not of MDPI and/or the editor(s). MDPI and/or the editor(s) disclaim responsibility for any injury to people or property resulting from any ideas, methods, instructions or products referred to in the content.